A NUMERICAL INVESTIGATION OF THE WHITHAM EQUATION FOR SOLITARY WAVES PROPAGATING ON CONDUCTING FLOWS

by MARCEL SOUZA

(UFPR/Federal University of Paraná, Departamento de Matemática, Centro Politécnico, Jardim das Américas, Caixa Postal 19081, Curitiba, PR 81531-980, Brazil)

MARCELO V. FLAMARION

(Sección Matemáticas, Departamento Académico de Ciencias, Pontificia Universidad Católica del Perú, Av. Universitaria 1801, San Miguel, Lima 15088, Peru)

ROBERTO RIBEIRO-JR

(UFPR/Federal University of Paraná, Departamento de Matemática, Centro Politécnico, Jardim das Américas, Caixa Postal 19081, Curitiba, PR 81531-980, Brazil)

and

TAO GAO[†]

(School of Mathematics, Statistics and Actuarial Science, University of Essex, Colchester CO4 3SQ, UK)

[Received September 18, 2025. Revised January 16, 2026. Accepted January 21, 2026]

Summary

We introduce the Whitham equation in the context of electrohydrodynamic (EHD) flows, which incorporates the nonlinearity of the Korteweg-de Vries (KdV) and the full linear dispersion relation associated with EHD effects, extending the classical Whitham approach to electrical regimes. This EHD extension will be referred to as the e-Whitham equation. To assess its performance, we conduct numerical simulations comparing the e-Whitham equation to the Korteweg-de Vries-Benjamin-Ono (KdV-BO) across various electric field strengths. We investigate travelling wave profiles, solitary wave collisions, and trapped wave phenomena. The numerical experiments demonstrate strong agreement with asymptotic predictions. The model reduces to the KdV-BO equation in the weakly dispersive regime, confirming its consistency with known asymptotics and ensuring accuracy where asymptotic models are valid. Its main novelty lies in extending the Whitham framework to EHD flows, making it suitable for exploring parameter regimes beyond the reach of KdV-BO.

1. Introduction

The study of water waves has been a subject of interest since the earliest days of science. Due to the physical complexity involved, mathematical models require simplifying assumptions, and different choices of these assumptions lead to different models. The fundamental one is the Euler equations, formulated in the 18th century by Leonhard Euler, which treat water as an inviscid, incompressible fluid and obey the principles of mass and momentum conservation.

[†]Corresponding author <t.gao@essex.ac.uk>

Q. Jl Mech. Appl. Math, Vol. 79. No. 2 © The Author, 2026. Published by Oxford University Press.

https://doi.org/10.1093/qjmam/hbag003

The Euler equations form a nonlinear system of partial differential equations with a free, moving boundary, making both analytical and numerical studies challenging. Reduced models typically rely on parameters representing nonlinearity and dispersion, and asymptotic expansions are performed in various regimes, such as weak nonlinearity without dispersion assumptions (**1**), shallow water without nonlinearity restrictions (**2**, p. 156), or balanced nonlinearity and dispersion as in the KdV model (**3**).

As George E. P. Box (**4**) famously stated, "all models are wrong, but some are useful." This applies well to the KdV equation, which is useful but fails to capture phenomena like wave breaking and the formation of peaked waves. To address these limitations, Gerald B. Whitham, (5, 6) proposed a model that retains the nonlinearity of the KdV equation but incorporates the full linear dispersion relation from the Euler equations. This Whitham equation extends the range of frequencies considered, increasing the model's validity while remaining mathematically tractable. Moreover, a known limitation of the KdV model, namely that waves propagate backwards withinfinite speed in the short-wave limit, is rectified by the Whitham equation [(7)]. Although *ad hoc*, it provides a better framework for capturing complex wave phenomena.

The Whitham equation performs well in capturing phenomena like wave breaking and peaked waves seen in full Euler dynamics (**8**). It combines shallow water nonlinearity with full linear dispersion relation from the Euler Equations through a convolution kernel defined by the inverse Fourier transform of the phase velocity. Research on the Whitham equation splits into analytical studies—including derivation of the model (**7**, **9**, **10**, **11**), existence (**12**, **13**, **14**), wave breaking (**15**) and regularity results (**16**)—and numerical investigations—focusing on solitary wave collisions (**17**), trapped waves (**18**, **19**, **20**), stability (**21**) and comparisons with other models (**7**, **9**, **13**, **22**).

EHD phenomena typically concern an interface between two fluids, which have applications in advanced coating processes, electrostatic thin film radiators (**23**), and cooling systems (**24**), underscoring the need for models in this field. The readers are referred to (**25**, **26**) for a review. Various physical configurations were considered in the literature. The most general configuration involves two immiscible dielectric liquids of different depths, densities and electric permittivities, separated by an interface. In previous studies, additional assumptions were typically introduced to simplify this complex problem. For example, the upper fluid is often assumed to have zero density, corresponding to a gas layer, while both layers are still treated as dielectric, as discussed in Ref. (**27**). A further assumption, frequently introduced in the literature, is that the lower (liquid) layer is perfectly conducting, while the upper (gas) layer is perfectly dielectric. This configuration closely reflects practical settings and is also adopted in the present study. In this context, various weakly nonlinear models have been derived. Glesson *et al.* (**28**) derived a KdV-BO model for the interfacial dynamics, incorporating the Hilbert transform to describe dispersion. Hunt and Vanden-Broeck (**29**) studied the electric effect on the fluid surface response due to a moving disturbance within a forced KdV-BO framework. Wang (**30**) has conducted a more comprehensive investigation of different model equations for three-dimensional space from the long-wave limit to the short-wave limit. A more recent work by Gao *et al.* (**31**) derived the NLS for waves on a conducting fluid of arbitrary depth. To the best of our knowledge, the Whitham-type equation has not yet been formulated for electrohydrodynamic (EHD) waves.

This work aims to address this gap by deriving the Whitham equation, which captures wave behaviour under electric fields across a broader depth regime, extending the range of validity from long waves, as modelled by the standard KdV-BO equation, to short waves, described by the NLS. The model is referred to as the e-Whitham equation in the rest of this work. Starting from the Euler equations for EHD flows, we linearise the system to obtain phase velocities

and integrate these into the KdV-BO framework to formulate the e-Whitham model. Numerical experiments, using pseudo-spectral methods, are conducted to investigate the proposed model by comparing its solutions with those of the KdV-BO. Additionally, we analyse travelling waves, solitary wave collisions and trapped waves under varying electric field strengths.

The study is organised as follows: first, the mathematical formulation and derivation of the e-Whitham equation are presented; next, the subsequent section explores numerical experiments on travelling waves, solitary wave collisions and trapped waves; finally, conclusions are drawn.

2. Formulations

We consider a two-dimensional, incompressible, irrotational flow of a perfectly conducting inviscid fluid with depth h_0. This fluid is bounded below by an electrode wall and above by an infinite layer of dielectric gas with permittivity $\bar{\varepsilon}$. The Cartesian coordinate system (x,y) is introduced such that gravity g acts in the negative y-direction. The interface between the fluid and the gas is free to move and will be called the free surface. Without loss of generality, we assume the electrode wall is at $y = 0$ and the free surface is at $y = h_0 + \eta(x,t)$. The fluid motion is described by the velocity potential $\phi(x,y,t)$, which satisfies the Laplace equation in the region $0 < y < h_0 + \eta(x,t)$, referred to as region 1. We denote by σ the surface tension on the free surface.

An electric field $\vec{E}$ acts vertically in the region occupied by the dielectric gas, that is, $y > h_0 + \eta(x,t)$, called region 2. For simplicity, it is assumed that the electric field is static, and the induced magnetic field is negligible. Maxwell equations then imply $\nabla \times \vec{E} = 0$. Thus, it is possible to introduce an electric potential V such that $\vec{E} = \nabla V$, and V satisfies the Laplace equation in region 2. Since the fluid in region 1 is perfectly conducting, we may set $V = 0$ in that region without losing generality. Consequently, $V = 0$ at $y = 0$. A vertical electric field is imposed by assuming $V \sim E_0 y$ as $y \to +\infty$, where E_0 is a constant. Figure 1 schematically illustrates the described problem.

By selecting the characteristic velocity $c_0 = \sqrt{gh_0}$, the characteristic amplitude a of the free surface, and the characteristic length l, we define the nondimensional variables according to Gleeson *et al.* (**28**) as:

$$\begin{aligned} &x = lx', \quad t = \frac{l}{c_0}t', \quad \eta = a\eta', \quad \phi = \frac{gla}{c_0}\phi', \quad y^{(1)} = h_0 y', \\ &y^{(2)} = lY', \quad V = lE_0 V', \quad \alpha = \frac{a}{h_0}, \quad \beta = \frac{h_0^2}{l^2}. \end{aligned} \tag{2.1}$$

Here, $y^{(1,2)}$ denotes the vertical coordinates in regions 1 and 2, respectively, α is the amplitude parameter that measures the nonlinearity, and β is the depth parameter of the problem that determines the type of regime, for example, shallow-water, deep-water.

Using the nondimensional variables in (2.1), we present the governing Euler equations and boundary conditions in nondimensional form as given by Gleeson *et al.* (**28**) (for simplicity, primes are omitted):

$$\beta\phi_{xx} + \phi_{yy} = 0, \qquad 0 < y < 1 + \alpha\eta, \tag{2.2}$$

$$V_{xx} + V_{YY} = 0, \qquad Y > \sqrt{\beta}(1 + \alpha\eta), \tag{2.3}$$

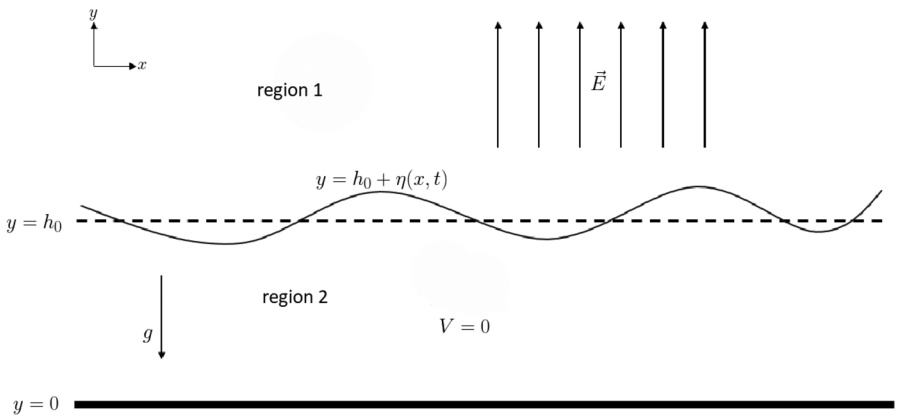

Fig. 1 Schematic description of the problem

$$\eta_t + \alpha\phi_x\eta_x - \frac{1}{\beta}\phi_y = 0, \qquad y = 1 + \alpha\eta, \tag{2.4}$$

$$V_x + \alpha\sqrt{\beta}\eta_x V_Y = 0, \qquad Y = \sqrt{\beta}(1 + \alpha\eta), \tag{2.5}$$

$$\phi_y = 0, \qquad y = 0, \tag{2.6}$$

$$V_Y \to 1, \qquad Y \to +\infty, \tag{2.7}$$

$$\begin{aligned}\phi_t + \frac{1}{2}\left(\alpha\phi_x^2 + \frac{\alpha}{\beta}\phi_y^2\right) + \eta \\ + \frac{E_b}{\alpha(1+\alpha^2\beta\eta_x^2)}\left[-\frac{1}{2}(V_Y^2 - V_x^2)(1-\alpha^2\beta\eta_x^2) + 2\alpha\sqrt{\beta}\eta_x V_x V_Y\right] \\ = \beta\tau\frac{\eta_{xx}}{(1+\alpha^2\beta\eta_x^2)^{3/2}} + C, \quad y = 1 + \alpha\eta,\end{aligned} \tag{2.8}$$

where C is a constant, $E_b = \frac{\bar{\varepsilon}E_0^2}{\rho g h_0}$ is the electric Froude number, and $\tau = \frac{\sigma}{\rho g h_0^2}$ is the Bond number. The electric Froude number measures the ratio of the electric field force to gravity, while the Bond number measures the ratio of capillarity to gravity.

2.1. *Linear theory*

For seeking linear travelling wave solutions, we perturb the trivial solution by

$$\eta = \varepsilon\tilde{\eta}, \quad \phi = \varepsilon\tilde{\phi}, \quad V = Y + \varepsilon\tilde{V}, \quad C = C_0 + \varepsilon\tilde{C}, \tag{2.9}$$

with small parameter $\varepsilon > 0$ and $C_0 = -\frac{E_b}{2\alpha}$. By using the ansatz

$$\tilde{\eta}(x,t) = \Re\{Ae^{i(kx-\omega t)}\}, \tag{2.10}$$

in which A is the amplitude, ω is the angular frequency and k is the wavenumber in the governing equations, it can be obtained that the linear wave phase speed c_F is written by

$$c_F^2 = \left(\frac{1}{\sqrt{\beta}k} - \mathrm{sgn}(k)E_b + \sqrt{\beta}\tau k\right)\tanh(k\sqrt{\beta}). \tag{2.11}$$

We note that c_F is guaranteed to admit a real solution provided that

$$E_b \leqslant 2\sqrt{\tau}. \tag{2.12}$$

When $E_b > 2\sqrt{\tau}$, the right-hand side of (2.11) may become negative for some k, which results in a destabilised fluid system.

2.2. *KdV-BO equation*

From the nondimensional system (2.2)-(2.8), Gleeson *et al.* (**28**) derived the KdV-BO equation under the assumption that $\alpha = \beta = \epsilon \ll 1$, which can be written by

$$\eta_T + \frac{3}{2}\eta\eta_X + \frac{1}{2}\left(\frac{1}{3} - \tau\right)\eta_{XXX} - \frac{1}{2}\gamma\mathcal{H}[\eta_{XX}] = 0, \tag{2.13}$$

where $T = \beta t$, $X = x - t$, $\gamma = E_b/\sqrt{\beta}$ and $\mathcal{H}$ is the Hilbert transform defined in Fourier space by

$$\widehat{\mathcal{H}[f]} = -i\,\mathrm{sgn}(k)\hat{f}(k).$$

Linearising (2.13) and using the ansatz $\tilde{\eta}(X,T) = e^{i(kX-\omega T)}$ and the Hilbert transform property, the dispersion relation follows as

$$c_B = \frac{k^2}{2}\left(\tau - \frac{1}{3}\right) - \frac{\gamma|k|}{2}. \tag{2.14}$$

It is worth noting that, upon transforming the variables back to x and t, the linear phase speed becomes $1 - \beta\left(\frac{\gamma|k|}{2} + \frac{k^2}{2}\left(\frac{1}{3} - \tau\right)\right)$ which can also be obtained by expanding c_F from (2.11) around $k = 0$ up to the quadratic order.

In the absence of the electric fields, (2.13) reduces to the standard KdV equation, which allows depression solitons for $\tau > 1/3$ and elevation solitons for $\tau < 1/3$. The differential equation becomes invalid in the critical case where $\tau = 1/3$, and a fifth-order model is usually derived for further investigation. In the present context where γ is non-zero, (2.13) does not collapse when $\tau = 1/3$ thanks to the term in Hilbert transform due to the electric effects, that is, in theory, elevation and depression solitary waves may exist beyond the limiting value.

2.3. *Electrified Whitham equation*

With the full linear dispersion relation (2.11), we define the electrified Whitham equation using the same coordinates as in the KdV-BO equation (2.13) as follows

$$\eta_T + \frac{3}{2}\eta\eta_X + \mathcal{K} * \eta_X = 0, \tag{2.15}$$

where the Fourier symbol $\hat{\mathcal{K}}(k)$ is written by

$$\hat{\mathcal{K}}(k) \equiv c_W(k) = \frac{1}{\beta}\left(\sqrt{\left(\frac{1}{\sqrt{\beta}k} - \mathrm{sgn}(k)\gamma\sqrt{\beta} + \sqrt{\beta}\tau k\right)\tanh(k\sqrt{\beta})} - 1\right). \tag{2.16}$$

In particular, the presence of a minus one at the end in (2.16) is due to the selection of a reference frame moving with the long-wave speed (scaled to be 1). The appearance of the factor $1/\beta$ on the right-hand side of (2.16) is to balance the slow time variable T ($= \beta t$). The restriction of the E_b in (2.12) now reads

$$\gamma \leqslant 2\sqrt{\frac{\tau}{\beta}} \tag{2.17}$$

which is satisfied in all the subsequent computations.

2.4. *Numerical scheme*

The spatial derivatives in the equations are computed numerically using the Fast Fourier Transform (FFT), denoted by $\mathcal{F}$. The Hilbert transform can then be computed by

$$\mathcal{H}[.] = \mathcal{F}\big[-i\mathrm{sgn}(k)\,\mathcal{F}[.]\big]. \tag{2.18}$$

Time integration of the governing equation is carried out using the classical fourth-order Runge–Kutta method, with timestep ΔT which is set to be 0.01.

For travelling waves, the governing equation is reduced to an ordinary differential equation as all functions depend on $X - cT$, which is solved by Newton's method. We denote A by the wave amplitude, which is defined by

$$A = \max_X(|\eta(X)|). \tag{2.19}$$

With a continuation strategy over parameters A and E_b, highly nonlinear solutions can be obtained. In all experiments presented in this section, we consider a computational domain with $N = 2^{12}$ grid points and spatial step size $\Delta X = 0.1$. The residual error is set to be at the order of 10^{-10}.

3. Results

We conducted numerical simulations to evaluate the performance of the e-Whitham model in comparison to the KdV-BO. The simulations focus on three main phenomena: travelling waves, solitary wave collisions, and trapped wave behaviour.

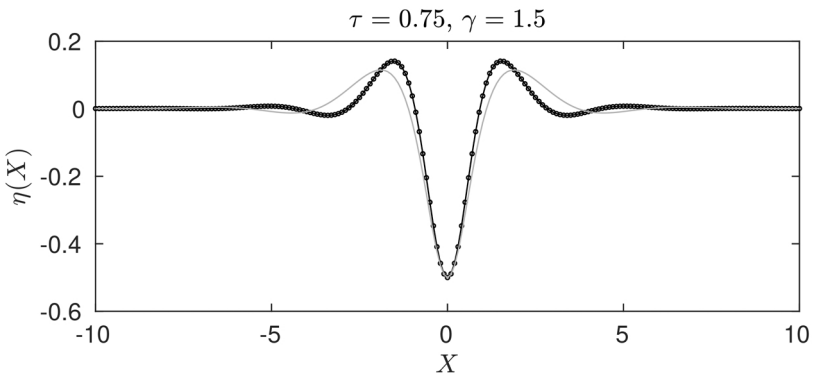

Fig. 2 Comparison between the depression solitary waves of e-Whitham equation with $\beta = 0.0001$ (black solid curve) and $\beta = 0.3$ (grey curve) for $\gamma = 1.5$, $\tau = 0.75$ and $A = 0.5$. The associated depression wave advised by the KdV-BO equation is marked in circles.

3.1. *Depression waves*

First, we investigate depression waves. In all the experiments considered in this context, we fix $\tau = 0.75$ and $A = 0.5$. Figure 2 displays the first experiment, where we set $\gamma = 1.5$. We observe that, for small values of β, the travelling wave solution of the e-Whitham equation closely approximates the solution of the KdV-BO equation. As the parameter β increases, however, the e-Whitham solution gradually departs from that of the KdV-BO, due to the difference in dispersive effect caused by $\mathcal{K}$ from (2.16). To further illustrate this difference, Fig. 3 presents a direct comparison of the linear dispersion relations associated with the e-Whitham equation (2.16) and the KdV–BO equation (2.14) for different values of β. It can be seen that, for sufficiently small β, the two dispersion relations are nearly indistinguishable, while noticeable deviations arise as β increases. We recall that, unlike the KdV–BO equation, which is derived under the long-wave assumption $\beta \ll 1$ and is therefore valid only in this asymptotic regime, the e-Whitham equation incorporates the full linear dispersion relation of the Euler equations. We further validate the e-Whitham equation by comparing its solutions with those obtained from the full Euler equations. Travelling depression solitary waves are computed using the numerical scheme described in (**31**) and subsequently rescaled to the present nondimensional framework. As shown in Fig. 4, the agreement between the Whitham model and the full Euler Equations is very good for $\beta = 0.05$, corresponding to the intermediate-depth regime. However, noticeable discrepancies are observed for $\beta = 0.3$, which represents the deep-water case. These numerical results indicate that the Whitham model provides an effective description of wave behaviour beyond the long-wave limit, however its applicability in the deep-water regime may still be restricted.

Figure 5 shows the wave profiles of depression waves when β is fixed to be 0.05 for various values of γ. It can be seen that the dispersion becomes stronger as the electric effect increases, leading to the appearance of decaying oscillatory ripples. A further increase in γ results in a solitary wavepacket-like solution. This behaviour can be understood by examining the linear phase speed: as illustrated in Fig. 8 (left panel), increasing γ leads to the formation of a local

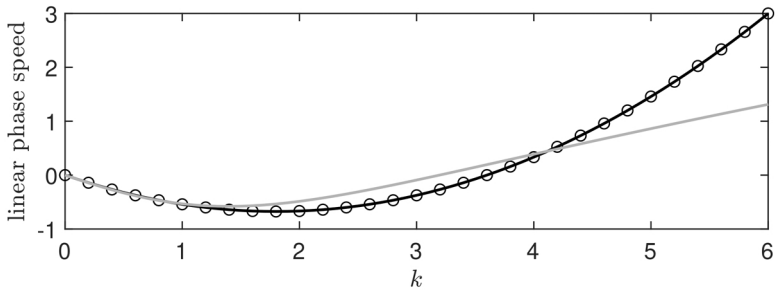

Fig. 3 Comparison of the linear dispersion relations associated with the KdV–BO equation (2.14) (marked by circles) and the e-Whitham equation (2.16) for $\beta = 0.0001$ (black solid curve) and $\beta = 0.3$ (grey curve) for $\gamma = 1.5$, $\tau = 0.75$.

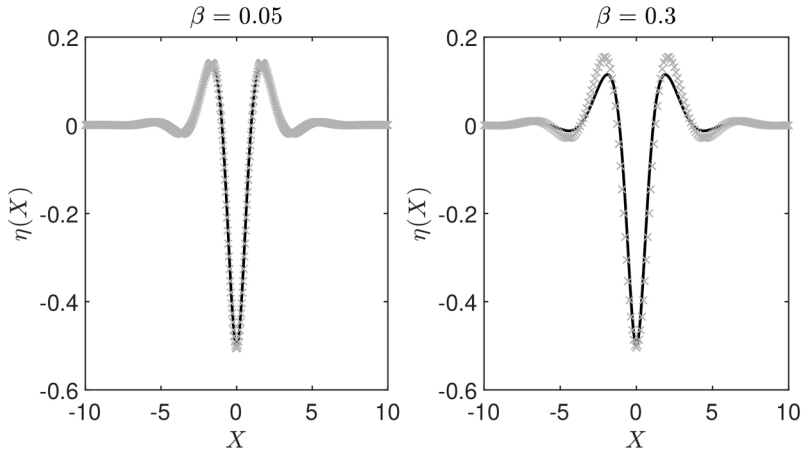

Fig. 4 Comparison between the depression solitary waves computed by the e-Whitham equation (solid black curves) and the full Euler Equations (grey crosses) for $\beta = 0.05$ (left) and $\beta = 0.3$ (right).

minimum of the linear phase speed at a finite wavenumber. Such a minimum provides the necessary condition for the bifurcation of solitary wavepacket solutions.

In Fig. 6, the wave speed is shown as a function of the electric Froude number γ. We note that, as γ increases, the wave speed c decreases. The e-Whitham wave speed almost coincides with the KdV-BO speed (circles) when β is close to zero, as expected from the theory. When β is further increased, a significant difference is observed for large γ, corresponding to strong electric fields.

3.2. *Elevation waves*

Secondly, we analyse the influence of the electric field on elevation waves with capillarity. In the experiments conducted for this section, we set $\tau = 0.25$ and $A = 0.5$.

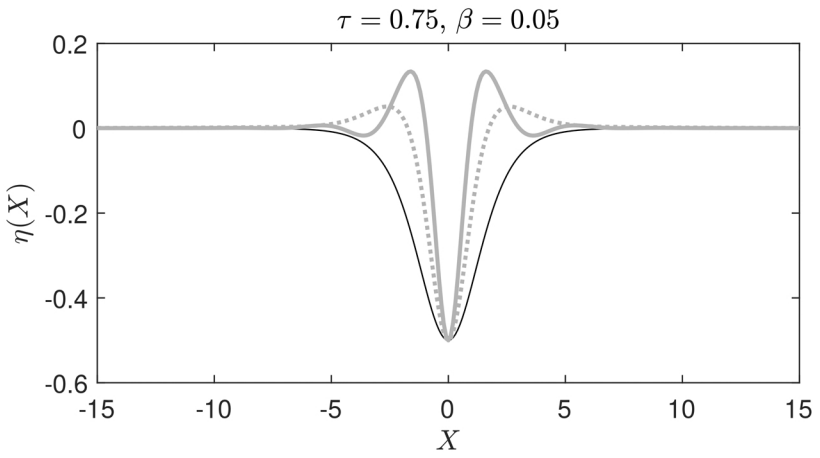

Fig. 5 The e-Whitham depression solitary waves with $\beta = 0.05$, $\tau = 0.75$ and $A = 0.5$ for various values of γ. The black solid curve corresponds to $\gamma = 0$, the grey dashed curve to $\gamma = 0.75$, and the grey solid curve to $\gamma = 1.5$.

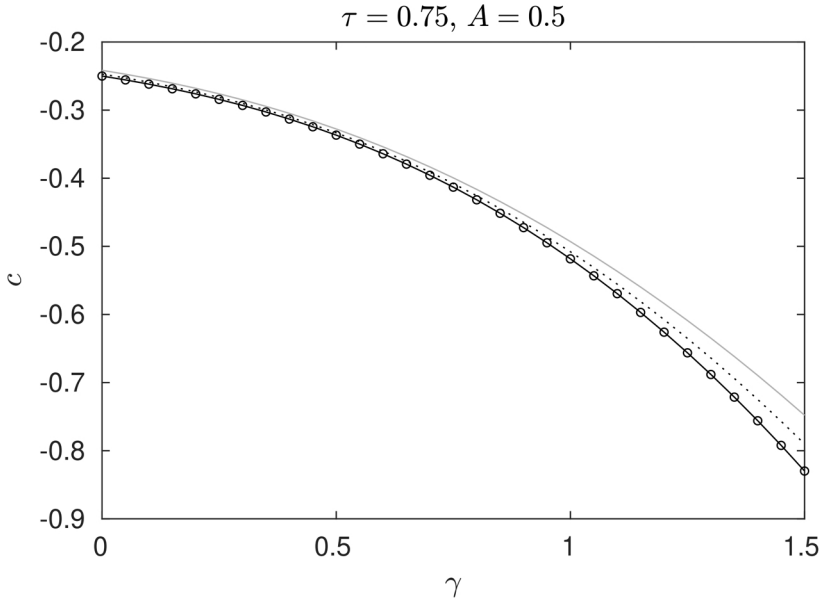

Fig. 6 Wave speed as a function of the electric Froude number γ for $\tau = 0.75$ and $A = 0.5$, in the case where $\beta = 0.0001$ (black solid curve), $\beta = 0.1$ (dotted curve) and $\beta = 0.3$ (grey solid curve). The prediction by the KdV-BO equation is marked by circles.

Fixing $\gamma = 1.5$, elevation waves are computed in the e-Whitham regime for various values of β. They closely match the KdV-BO solution. One example is presented in Fig. 7. For larger

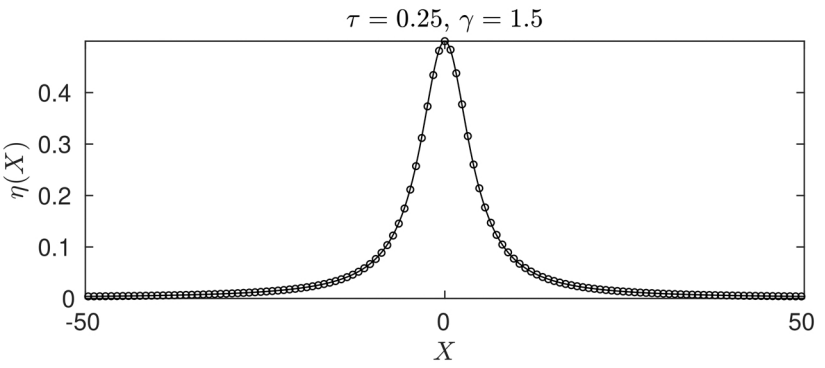

Fig. 7 Comparison between the travelling wave solutions of the e-Whitham equations (black solid curve) with $\beta = 0.02$ and the KdV-BO (circles) in the case where $\gamma = 1.5$, with $\tau = 0.25$ and $A = 0.5$.

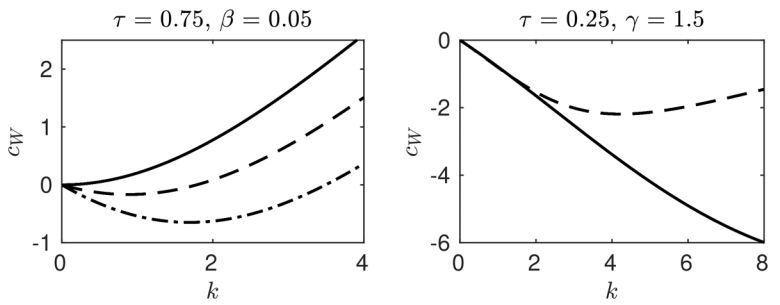

Fig. 8 Left: linear wave phase speed c_W as a function of the wavenumber k for $\gamma = 0$ (solid line), $\gamma = 0.75$ (dashed line), and $\gamma = 1.5$ (dot–dashed line), with $\tau = 0.75$ and $\beta = 0.05$. Right: linear wave phase speed c_W for $\beta = 0.02$ (solid line) and $\beta = 0.2$ (dashed line), with $\tau = 0.25$ and $\gamma = 1.5$.

values of β, however, the numerical method becomes very sensitive and fails to converge. One possible reason is that the elevation wave resonates with periodic waves in the case of finite depth and turns to be a generalised solitary wave, which the numerical scheme can no longer deal with. This interpretation is supported by Fig. 8 (right panel), where the linear phase speed develops a local minimum at a finite wavenumber as β increases, providing the necessary condition for resonance between solitary and periodic waves.

A comparison of the elevation waves for various values of γ is displayed in Fig. 9. Increasing the electric field intensity strengthens the dispersion effect, resulting in broader solitary wave profiles.

It is observed that increasing γ causes a decrease in the wave speed c, as shown in Fig. 10. The wave speeds for various γ exhibit significant differences in the absence of the electric field and tend to a limit value as γ approaches 1.5, illustrating the fact that the electric effect may dominate the depth effect measured by β in this context.

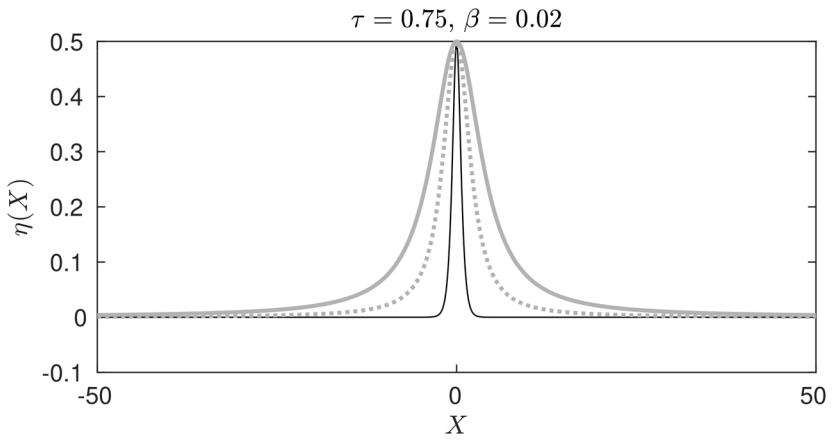

Fig. 9 Comparison of travelling wave profiles for different values of γ: $\gamma = 0$ (black solid curve), $\gamma = 0.75$ (grey dotted curve), $\gamma = 1.5$ (grey solid curve) in the e-Whitham framework with $\beta = 0.02$, $\tau = 0.25$ and $A = 0.5$.

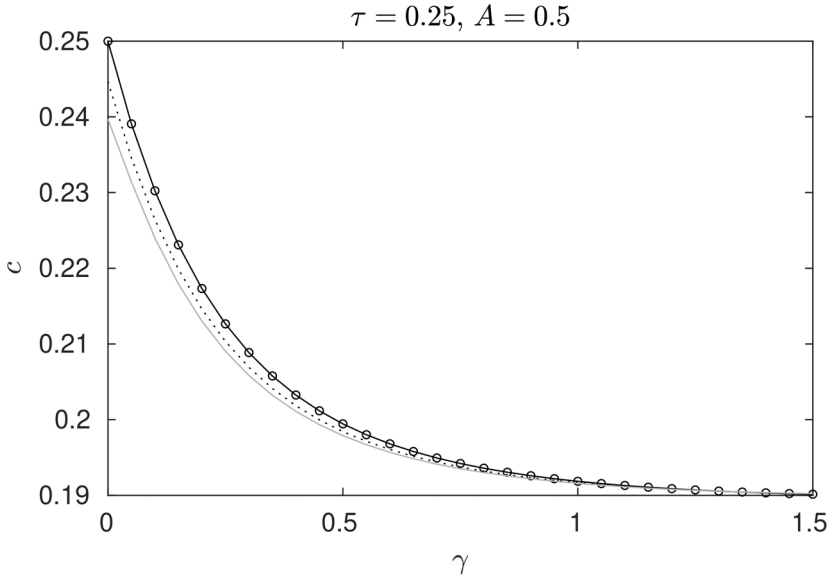

Fig. 10 Wave speed as a function of the electric Froude number γ for $\tau = 0.25$ and $A = 0.5$, in the case where $\beta = 0.0001$ (black solid curve), $\beta = 0.02$ (dotted curve) and $\beta = 0.03$ (grey solid curve). The prediction by the KdV-BO equation is marked by circles.

The classical KdV theory predicts a critical value of τ due to a change of sign in the dispersive term. However, this is no longer applicable in the e-Whitham regime, that is, elevation waves may exist for $\tau > 1/3$ and depression waves may exist for $\tau < 1/3$. By a continuation method

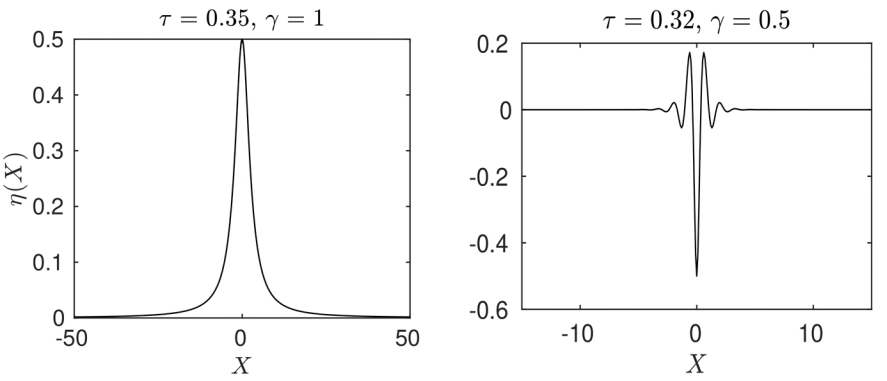

Fig. 11 Solitary waves beyond the critical value $\tau = 1/3$. (Left) An elevation wave with $\gamma = 1$ and $\tau = 0.35$ computed in the e-Whitham regime with $\beta = 0.05$. (Right) A depression wave with $\gamma = 0.5$ and $\tau = 0.32$ computed in the e-Whitham regime with $\beta = 0.05$.

over the value of τ, elevation waves and depression beyond the critical value are discovered and demonstrated in Fig. 11. The same argument also stands in the KdV-BO framework, whose results are shown in Appendix A.

If the absence of capillarity, that is, $\tau = 0$, the results are qualitatively similar to those discussed above. In summary, we observed that the solution of the e-Whitham equation closely approximates the KdV-BO solution as $\beta \to 0$, in agreement with the asymptotic approximation presented in the previous section. Moreover, in all scenarios analysed, we observed that the wave speed c decreases as the electric Froude number γ increases, although the rate of this decay varies depending on the value of τ.

3.3. *Solitary wave collisions*

The goal of this section is to investigate the behaviour of solitary wave collisions involving travelling wave solutions of (2.15). Here, we focus exclusively on elevation waves without capillarity, that is, with $\tau = 0$ in the intermediate depth regime with $\beta = 0.05$ (the ratio of depth over wavelength is about 0.224) in which the KdV regimes may become invalid. For each experiment, we define two solitons S_1 and S_2 with amplitudes A_1 and A_2, respectively, where $A_1 < A_2$. These waves are initially placed far apart so that two distinct crests are well defined. From this point onward, for notational convenience, we denote x and t in place of X and T, respectively. The initial condition is given by:

$$\eta(x,0) = S_1(x + 10) + S_2(x - 20).$$

Lax (**32**) classified solitary wave collisions for the KdV equation both geometrically and algebraically. He introduced three categories— **(A)**, **(B)**, and **(C)**— as follows:

(A) For $\dfrac{A_2}{A_1} < \dfrac{3+\sqrt{5}}{2} \approx 2.62$, the collision between two solitary waves exhibits two local maxima at all times.

Table 1 Categorisation of wave solutions of the Whitham-BO equation.

A_1	A_2	A_2/A_1	Category
0.080	0.250	3.125	A
0.080	0.260	3.250	B
0.120	0.390	3.250	A
0.120	0.400	3.333	B
0.080	0.290	3.625	B
0.080	0.300	3.750	C
0.160	0.600	3.750	B
0.160	0.610	3.813	C

(B) For $\frac{3+\sqrt{5}}{2} < \frac{A_2}{A_1} < 3$, the collision undergoes a sequence of changes in the number of local maxima:

$$2 \to 1 \to 2 \to 1 \to 2.$$

This means that the waves initially form two separate crests, then merge into a single crest, separate again, merge once more, and finally split into two distinct crests again.

(C) For $\frac{A_2}{A_1} > 3$, the collision leads to a simpler sequence:

$$2 \to 1 \to 2.$$

That is, the two waves merge into a single crest for a brief time and then separate again.

We aim to classify the solitary wave collisions governed by the e-Whitham equation to address the following questions:

1. Is there a geometric classification of these collisions? If so, does it match the one proposed by Lax for the KdV equation?
2. Is there an algebraic classification depending solely on the amplitude ratio $\frac{A_2}{A_1}$?

To answer these questions, we perform a series of numerical tests for a variety of values satisfying $A_1 < A_2$, using the following parameters: spatial step $\Delta X = 0.1$, number of grid points $N = 2^{12}$, time step $\Delta T = 0.01$, electric Froude number $\gamma = 0.5$, and $\beta = 0.05$. Figs 12 to 14 show representative results for categories **(A)**, **(B)**, and **(C)**, respectively.

In Table 1, it can be seen that there is no algebraic relation depending solely on the ratio A_2/A_1 that categorises each collision.

Suppose there exist values r_{AB} and r_{BC} such that:

- if $A_2/A_1 < r_{AB}$, then the collision is of category A;
- if $r_{AB} < A_2/A_1 < r_{BC}$, then the collision is of category B;

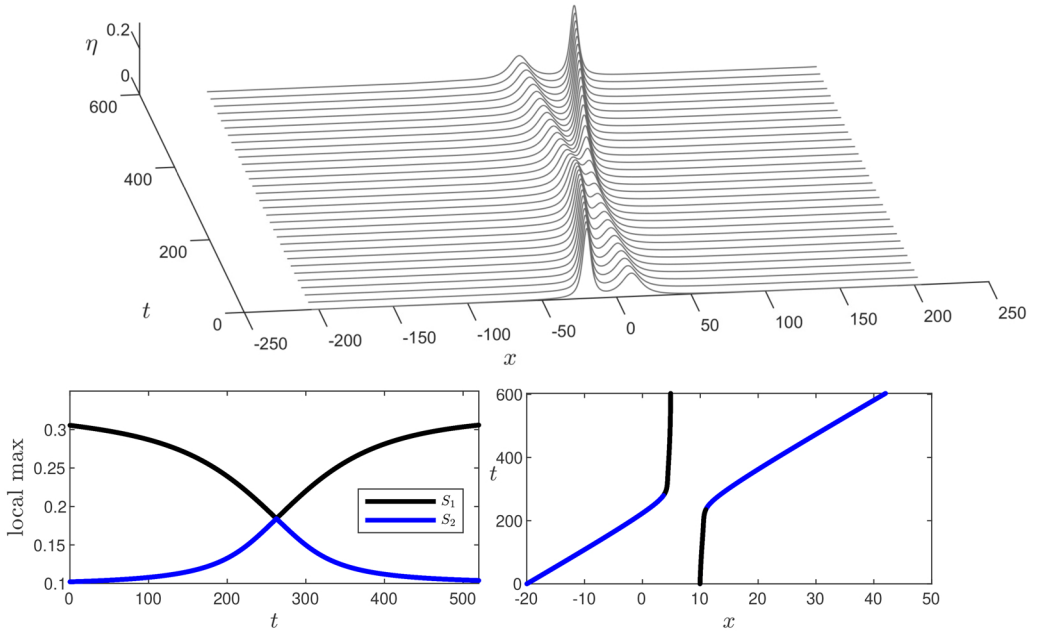

Fig. 12 Top: collision of two solitary wave solutions of the e-Whitham equation, classified as category **(A)**. Bottom left: the local maximum of the solution as a function of time. Bottom right: trajectories of the crests of each solitary wave over time. Parameters $A_1 = 0.1$, $A_2 = 0.3$.

- if $A_2/A_1 > r_{BC}$, then the collision is of category C.

Then r_{AB} and r_{BC} must satisfy:

$$3.125 < r_{AB} < 3.250 \quad \text{and} \quad 3.250 < r_{AB} < 3.333,$$
$$3.625 < r_{BC} < 3.750 \quad \text{and} \quad 3.750 < r_{BC} < 3.813.$$

This is clearly contradictory, demonstrating that such an algebraic relation cannot depend solely on the ratio A_2/A_1, likely due to the depth effect. However, it is possible to observe that the geometric classification defined by Lax is satisfied, as in the case of the wave solutions of the KdV-BO equation (see (33)).

In these experiments, we numerically studied the collisions of two solitary waves that are solutions of the e-Whitham equation. We found regimes in which the interactions of the waves maintain two well-separated crests at any instant, and regimes where the number of crests varies according to the sequences $2 \to 1 \to 2 \to 1 \to 2$ or $2 \to 1 \to 2$. We showed that Lax's geometric categorisation for the KdV equation still applies to the e-Whitham equation. However, we verified that an algebraic categorisation based only on the ratio of the initial amplitudes of the solitary waves cannot be established for the equation. It is interesting to note that the results obtained are in agreement with those found by Flamarion (34) in a similar study carried out for the Whitham equation.

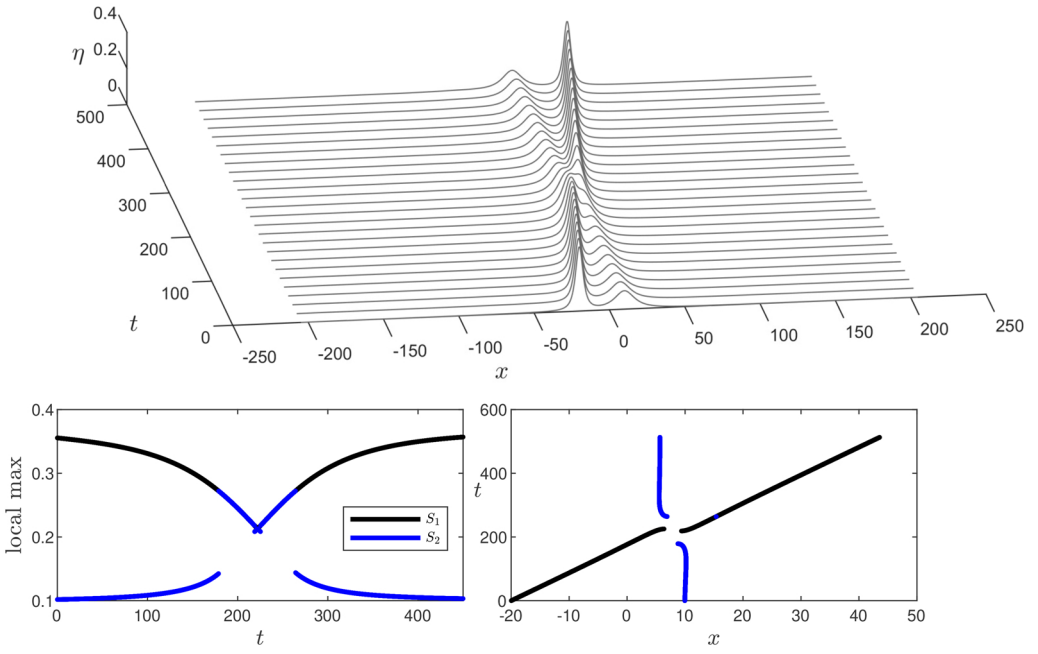

Fig. 13 Top: collision of two solitary wave solutions of the e-Whitham equation, classified as category **(B)**. Bottom left: the local maximum of the solution as a function of time. Bottom right: trajectories of the crests of each solitary wave over time. Parameters $A_1 = 0.1$, $A_2 = 0.35$.

3.4. *Trapped solitary waves*

In this section, we investigate the behaviour of solitary waves trapped between two elevations generated by a given non-uniform electrode wall. This type of study has already been carried out for the classical KdV equation [17, 35, 36, 37, 38] and for the standard Whitham equation [18, 19, 20].

The solitary waves considered in our study are the travelling wave solutions of the KdV-BO equation (2.13) and the e-Whitham model (2.15) with $\beta = 0.02$ (the ratio of depth over wavelength is about 0.141) corresponding to the intermediate depth regime. Through numerical simulations, we show that these solitary waves remain trapped, oscillating back and forth between the topographic obstacles $h(x)$, until they eventually escape. In these experiments, we employ an artificial damping layer $s(x)$ to absorb noise generated by wave transmission and reflection. To confirm that this sponge layer does not influence the wave dynamics, we include a dedicated test in Appendix B.

In this context, the forced KdV-BO equation and the forced e-Whitham equation can be written by

$$\eta_t - f\eta_x + \frac{3}{2}\eta\eta_x + \frac{1}{2}\left(\frac{1}{3} - \tau\right)\eta_{xxx} - \frac{1}{2}\gamma\mathcal{H}[\eta_{xx}] - s(x)\eta = -\frac{1}{2}h_x(x), \tag{3.1}$$

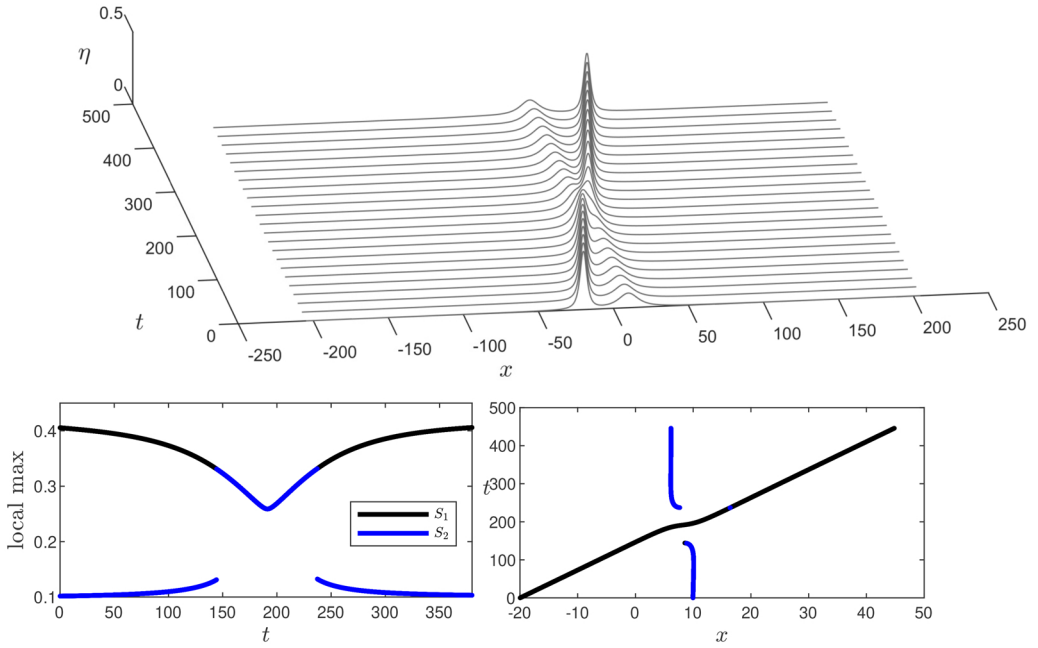

Fig. 14 Top: collision of two solitary wave solutions of the e-Whitham equation, classified as category **(C)**. Bottom left: the local maximum of the solution as a function of time. Bottom right: trajectories of the crests of each solitary wave over time. Parameters $A_1 = 0.1$, $A_2 = 0.4$.

and

$$\eta_t - f\eta_x + \frac{3}{2}\eta\eta_x + \mathcal{K} * \eta_x - s(x)\eta = -\frac{1}{2}h_x(x), \tag{3.2}$$

where $\hat{\mathcal{K}}(k)$ is advised in (2.16). The artificial damping function used in the simulations is given by

$$s(x) = \frac{a_1}{2}\Big(\tanh(x + a_2) - \tanh(x - a_2)\Big) - a_1,$$

where $a_1 = 10$ and $a_2 = 150$. The parameter a_1 controls the absorption strength, while a_2 determines the spatial extent of the damping region. The non-uniform electrode wall is modelled by

$$h(x) = \varepsilon\Big(e^{-(x-b)^2} + e^{-(x+b)^2}\Big),$$

with $\varepsilon = 0.01$ and $b = 40$. Here, ε determines the height of the elevations, and b controls their positions along the x-axis.

In the simulations, we fix the amplitude of the travelling solitary wave to $A = 0.5$. Let c_0 denote the wave speed in the absence of a non-uniform electrode wall. In this setting, choosing

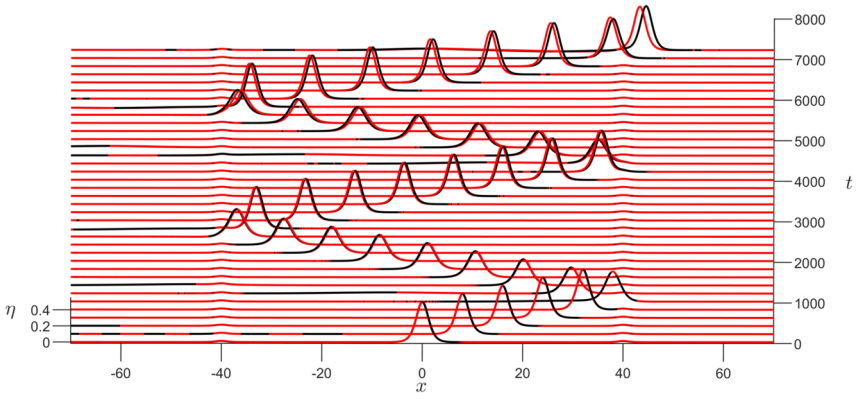

Fig. 15 Trapped solitary wave solutions of the forced e-Whitham equation (red) between two obstacles, for $\gamma = 0$. The prediction advised by the forced KdV-BO is depicted in black.

$f = c_0$ yields a stationary solution. According to Kim *et al.* (**36**), trapped waves can be characterised by their velocities: there exists a critical velocity threshold that a wave must exceed to overcome the topographic obstacles. Since kinetic energy is proportional to the square of the velocity, this threshold may be interpreted as an energy barrier. To ensure that the wave remains trapped, we slightly perturb its velocity such that it does not possess enough energy to surpass the obstacles. Following the approach of Flamarion *et al.* (**35**), we take $f = c_0 - 0.04$. We then vary the electric Froude number γ to investigate how the intensity of the electric field influences the behaviour of the trapped wave.

We consider trapped wave solutions of (3.1) and (3.2), and we analyse two distinct cases:

- **Case 1:** In this case, the initial condition is given by $\eta(x,0) = \eta_1(x) + \eta_2(x)$, where $\eta_1(x)$ is the travelling wave solution of (2.13) (respectively, (2.15)) over a flat bottom, and $\eta_2(x)$ is the stationary solution. The inclusion of $\eta_2(x)$ is necessary to suppress spurious radiation effects.
- **Case 2:** In this case, the initial condition is $\eta(x,0) = \eta_0(x) + \eta_2(x)$, where $\eta_0(x)$ is the exact solitary wave solution of the classical KdV equation, and $\eta_2(x)$ is the stationary solution of (2.13) (respectively, (2.15)). This experiment allows us to examine how well the classical KdV solution adapts to the forced e-Whitham equation.

3.4.1. Case 1: perturbation of the travelling wave speed This series of experiments was conducted using the following parameters: $\tau = 0$, $\Delta x = 0.1$, $N = 2^{12}$, $\Delta t = 0.005$, and $\beta = 0.02$.

We performed simulations by varying the value of γ in order to understand how the electric field influences the behaviour of trapped waves. Figures 15 and 16 ($\gamma = 0$) and ($\gamma = 0.1$) show that changes in γ significantly affect the wave dynamics. When $\gamma = 0$, the waves scape out to the right, whereas for $\gamma = 0.1$ they scape out to the left. It can also be observed that there is little difference in shape and velocity between the solutions obtained from the KdV-BO and e-Whitham equations.

A more detailed investigation—considering a broader range of γ values—reveals that as γ increases, the escape time of the trapped wave initially grows, reaching a maximum (which we refer to as the critical escape time), and then decreases again. This behaviour is illustrated in

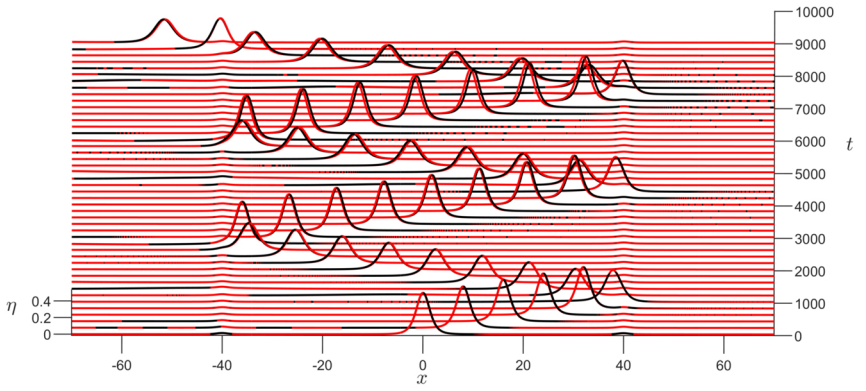

Fig. 16 Trapped solitary wave solutions of the forced e-Whitham equation (red) between two obstacles, for $\gamma = 0.1$. The prediction advised by the forced KdV-BO is depicted in black.

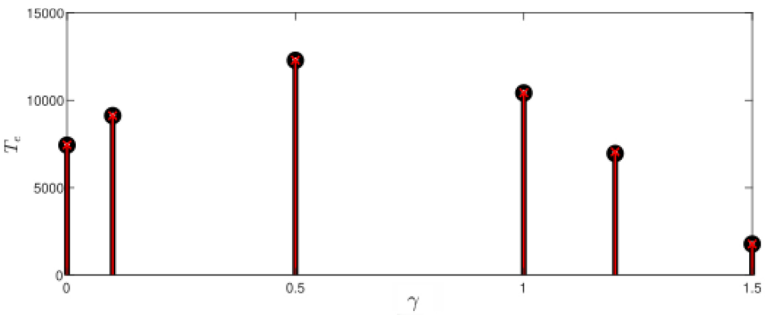

Fig. 17 Escape time T_e as a function of γ for wave solutions of the e-Whitham equation (red), in the context of Case 1. The predictions advised by the KdV-BO framework are marked in black.

Fig. 17. In the next section, we conduct a similar analysis following the approach described in Case 2. Meanwhile, it is also observed from the experiments that the crest height changes before escape: when the wave travels upstream, its amplitude increases until it reaches the obstacle; conversely, when it travels downstream, the amplitude decreases before reaching the obstacle.

3.4.2. Case 2: Classical KdV soliton in a flow with nonzero γ This experiment was carried out using the following parameters: $\tau = 0$, $\Delta x = 0.4$, $N = 2^{10}$, $\Delta t = 0.005$, and $\beta = 0.02$.

The goal is to investigate the behaviour of the solutions to (3.1) and (3.2) when initialised with the classical KdV solution. To this end, we tested several values of γ and recorded the corresponding escape time for each scenario, as shown in Fig. 18. We observe that, as γ increases, the escape time initially grows, reaching a critical value, and then begins to decrease. The critical escape time occurs for some value of γ in the interval [0.08,0.22].

In Fig. 18, we set an upper bound of 50000 for the escape time, but other experiments indicate that the critical escape time can exceed 150000. It is also noteworthy that the solutions of the forced KdV-BO and e-Whitham equations exhibit remarkably similar behaviour, even when using the maximum tested value of β.

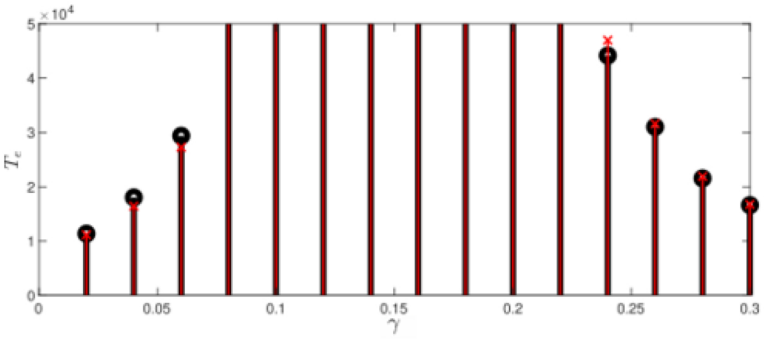

Fig. 18 Escape time T_e as a function of γ for wave solutions of the e-Whitham (red) equations, under Case 2. The predictions advised by the KdV-BO framework are marked in black.

In summary, our numerical results show that the trapped solitary wave solutions of the forced KdV-BO and e-Whitham equations oscillate between two collisions for a time that depends on the applied electric field. In other words, the escape time of the trapped waves is influenced by the strength of the electric field. We observed that the escape time increases up to a critical value and then decreases. Additionally, the difference in behaviour between the solutions of the KdV-BO and e-Whitham equations with $\beta = 0.02$ is insignificant.

4. Conclusion

This work presented the derivation of the e-Whitham equation and conducted numerical studies on travelling and trapped solitary wave solutions. We confirmed that the e-Whitham reduces to the KdV-BO equation as dispersion vanishes and observed numerical convergence of their solutions in this limit. Numerical experiments revealed that wave speed decreases with increasing electric Froude number, and novel solitary waves beyond the critical value $\tau = 1/3$ were discovered. We also investigated solitary wave collisions and found that, although an algebraic classification based solely on amplitude ratios is not possible for either the KdV-BO or the e-Whitham equations, a geometric classification analogous to Lax's framework can be established. Additionally, trapped waves were shown to oscillate for durations that depend on the electric field strength, with negligible differences between the two models.

Although the e-Whitham often reproduces KdV-BO behaviour, possibly because the depth effect could be dominated by the electric effect, this agreement should be seen as validation and generalisation rather than limitation, since it ensures accuracy where asymptotic models are valid. Its main novelty lies in extending the Whitham framework to EHD flows by incorporating the full linear dispersion relation, making it suitable to explore parameter regimes beyond the reach of KdV-BO. Future theoretical and numerical investigations will clarify the advantages of this new model and its role in understanding nonlinear EHD waves.

Acknowledgement

The work was completed during a visit by M. V. F. to the University of Essex, which was sponsored by a QJMAM Fund for Applied Mathematics (T. G. 2025). M.S. gratefully acknowledges the financial support from the CAPES Foundation (Coordination for the Improvement of Higher Education Personnel), which supported part of the development of

this work. R. R. Jr.'s work was partially supported by the National Council for Scientific and Technological Development (CNPq), under Grant No. 10/2023–Universal (CNPq/MCTI). T. G. thanks the London Mathematical Society for Grant Ref. 42432, which supported the visit of R. R. Jr. to the University of Essex.

References

1. G. G. Stokes, On the theory of oscillatory waves, *Trans. Cambridge Philos. Soc.* **8** (1847) 441–455.
2. L.Debnath, *Nonlinear Partial Differential Equations for Scientists and Engineers* (Birkhauser, Boston 2005).
3. D. J.KortewegG.de Vries, XLI. On the change of form of long waves advancing in a rectangular canal, and on a new type of long stationary waves, *Philos. Mag. J. Sci.* **39** (1895) 422–443.
4. G. E. P.BoxN. R.Draper, *Empirical Model-Building and Response Surfaces* (John Wiley & Sons, New York 1987).
5. G. B.Whitham, *Linear and Nonlinear Waves* (John Wiley & Sons, New York 1974).
6. Whitham G. B., Variational methods and applications to water waves, *Proc. R. Soc. Lond. A***299** (1967) 6–25.
7. D.MoldabayevH.KalischD.Dutykh, The Whitham equation as a model for surface water waves, *Physica D* **309** (2015) 99–107.
8. V. M.Hur, Wave breaking in the Whitham equation, *Adv. Math* **317** (2017) 410–437.
9. E.DinvayH.KalischD.MoldabayevE. I.Părău, The Whitham equation for hydroelastic waves, *Appl. Ocean Res.* **89** (2019) 202–210.
10. Ehrnström M., Nik K. and Walker C., A direct construction of a full family of whitham solitary waves, *Proc. Amer. Math. Soc.***151** (2023) 1247–1261.
11. L.Emerald, Rigorous derivation of the Whitham equations from the water waves equations in the shallow water regime, *Nonlinearity* **34** (2021) 7470–7509.
12. F. Hildrum, Solitary waves in dispersive evolution equations of Whitham type with nonlinearities of mild regularity, *Nonlinearity* **33** (2020) 1594–1624.
13. C. Klein, F. Linares, D. Pilod and J.-C. Saut, On Whitham and related equations, *Stud. Appl. Math.* **140** (2018) 133–177.
14. L. Pei and Y. Wang, A note on well-posedness of bidirectional Whitham equation, *Appl. Math. Lett.* **98** (2019) 215–223.
15. J.-C. Saut and Y. Wang, The wave breaking for Whitham-type equations revisited, *SIAM J. Math. Anal.* **54** (2022) 2295–2319.
16. Q. Miao and L. Xue, Regularity and singularity results for the dissipative Whitham equation and related surface wave equations, *Commun. Math. Sci.* **17** (2019) 2141–2190.
17. M. V. Flamarion, Rotational solitary wave interactions over an obstacle, *Trends Comput. Appl. Math.* **23** (2022) 531–538.
18. M. V. Flamarion, R. Ribeiro, Jr, D. L. S. S. Vianna and A. M. Sato, Trapped solitary waves in a periodic external force: a numerical investigation using the Whitham equation and the sponge layer method, *Fluids* **8** (2023) 223.
19. M. V. Flamarion, Trapped waves generated by an accelerated moving disturbance for the Whitham equation, *Partial Differ. Equat. Appl. Math.* **5** (2022) 100356.
20. M. V. Flamarion, Waves generated by a submerged topography for the Whitham equation, *Int. J. Appl. Comput. Math.* **8** (2022) 257.

21. J. D. Carter and M. Rozman, Stability of periodic, traveling-wave solutions to the capillary Whitham equation, *Fluids* **4** (2019) 58.
22. H. Borluk, H. Kalisch and D. P. Nicholls, A numerical study of the Whitham equation as a model for steady surface water waves, *J. Comput. Appl. Math*. **296** (2016) 293–302.
23. E. M. Griffing, S. G. Bankoff, M. J. Miksis and R. A. Schluter, Electrohydrodynamics of thin flowing films, *J. Fluids Engng* **128** (2006) 276–283.
24. U. Ghoshal and A. C. Miner. Cooling of high power density devices by electrically conducting fluids, U.S. Patent No. 6,658,861 (2003).
25. J. R. Melcher and G. I. Taylor, Electrohydrodynamics: a review of the role of interfacial shear stresses, *Annu. Rev. Fluid Mech.* **1** (1969) 111–146.
26. D. T. Papageorgiou, Film flows in the presence of electric fields, *Annu. Rev. Fluid Mech.* **51** (2019) 155–187.
27. A. Doak, T. Gao, J.-M. Vanden-Broeck and J. J. S. Kandola, Capillary-gravity waves on the interface of two dielectric fluid layers under normal electric fields, *Quart. J. Mech. Appl. Math*. **73** (2020) 231–250.
28. H. Gleeson, P. Hammerton, D. T. Papageorgiou and J.-M. Vanden-Broeck, A new application of the Korteweg–de Vries–Benjamin–Ono equation in interfacial electrohydrodynamics, *Phys. Fluids* **19** (2007) 031703.
29. M. J. Hunt and J.-M. Vanden-Broeck, A study of the effects of electric field on two-dimensional inviscid nonlinear free surface flows generated by moving disturbances, *J. Eng. Math.* **92** (2015) 1–13.
30. Z. Wang, Modelling nonlinear electrohydrodynamic surface waves over three-dimensional conducting fluids, *Proc. R Soc. A.* **473** (2017) 20160817.
31. T. Gao, Z. Wang and J.-M. Vanden-Broeck, Nonlinear wave interactions on the surface of a conducting fluid under vertical electric fields, *Physica D* **446** (2023) 133651.
32. P. D. Lax, Integrals of nonlinear equations of evolution and solitary waves, in *Selected Papers Volume* **I** (Springer, New York 2005),366–389.
33. M. Souza. A equação de Whitham-Benjamin-Ono: uma extensão do modelo de KdV-Benjamin-Ono, Master Thesis, Universidade Federal do Paraná (2024).
34. M. V. Flamarion, Solitary wave collisions for the Whitham equation, *Comput. Appl. Math*. **41** (2022) 356.
35. M. V. Flamarion, P. A. Milewski and R. Ribeiro-Jr. Trapped solitary waves and collisions for the forced Korteweg–de Vries equation, (2021) *arXiv:2109.06051*.
36. H. Kim and H. Choi, A study of wave trapping between two obstacles in the forced Korteweg–de Vries equation, *J. Engng. Math.* **108** (2018) 197–208.
37. S. Lee and S. Whang, Trapped supercritical waves for the forced KdV equation with two bumps, *Appl. Math. Model* **39** (2015) 2649–2660.
38. S. Lee, Dynamics of trapped solitary waves for the forced KdV equation, *Symmetry* **10** (2018) 129.

APPENDIX A

Solitary waves beyond the critical value $\tau = 1/3$ in the KdV-BO framework.

The solitary waves can be found beyond the critical value advised by the KdV regime by a continuation over τ as shown in Fig. 1A.

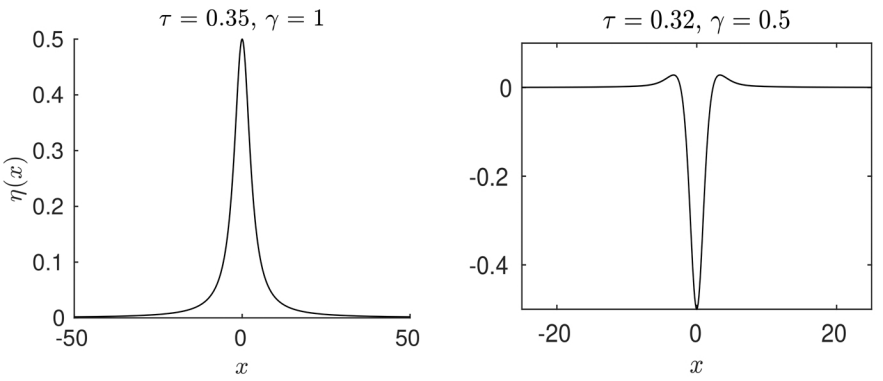

Fig. A1 Solitary waves beyond the critical value $\tau = 1/3$. (Left) Elevation waves with $\gamma = 1$ and $\tau = 0.35$ computed in the KdV-BO equation. (Right) Depression waves with $\gamma = 0.5$ and $\tau = 0.32$ computed in the KdV-BO equation.

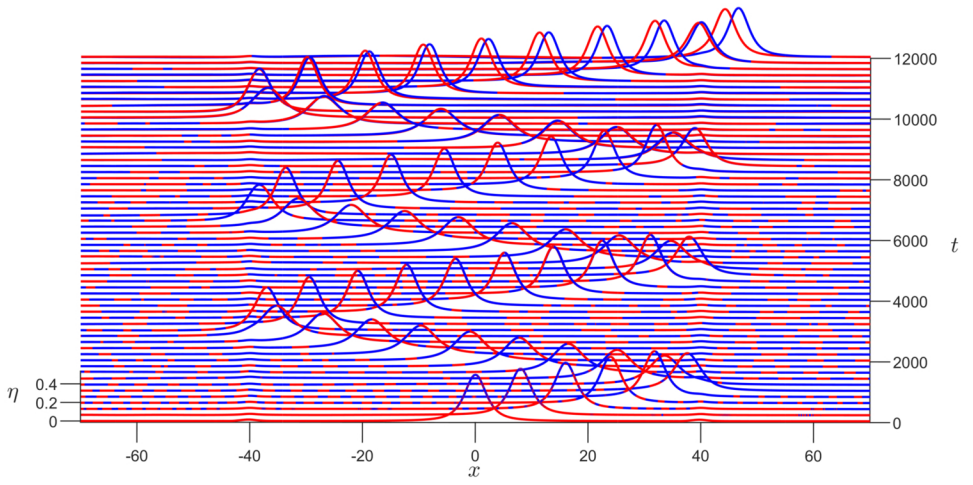

Fig. A2 Trapped waves, solutions of the KdV-BO equation with sponge (in red) and without sponge (in blue).

APPENDIX B

Influence of the Artificial Sponge.

Here, we present the artificial sponge layer employed in the numerical simulations and demonstrate that it does not affect the soliton by comparing numerical solutions obtained with and without the sponge layer.

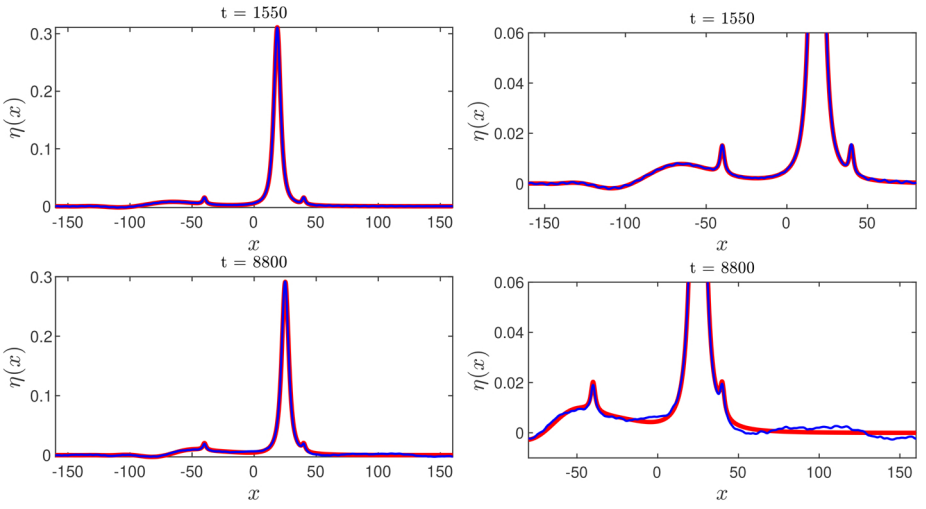

Fig. B1 Trapped waves, solutions of the KdV-BO equation with sponge (in red) and without sponge (in blue) at times $t = 1550$ (top left) and $t = 8800$ (bottom left). The zoom-in graphs are presented in the right panel.

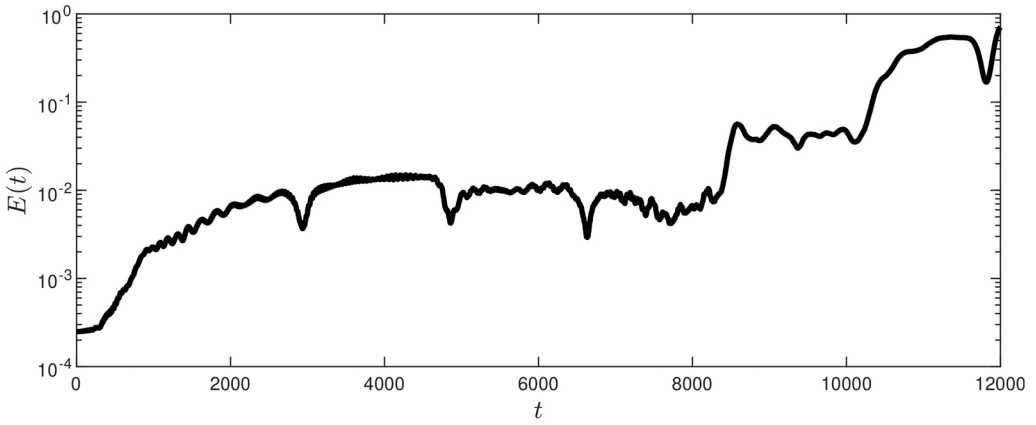

Fig. B2 Relative error $E(t)$ as a function of time t.

We examine in the framework of the forced KdV-BO equation with a sponge (the result for the e-Whitham regime is qualitatively similar), which is given by

$$\eta_t - f\eta_x + \frac{3}{2}\eta\eta_x + \frac{1}{2}\left(\frac{1}{3} - \tau\right)\eta_{xxx} - \frac{1}{2}\gamma\mathcal{H}[\eta_{xx}] - s(x)\eta = -\frac{1}{2}h_x(x). \tag{B.1}$$

The travelling and stationary waves used in the experiments are solutions of equation (B.1). For the numerical simulations, we use the following parameters:

- The computational domain in the case with sponge is $N_s = 2^{12}$, and in the case without sponge is $N_w = 2^{14}$.
- The spatial mesh step is $\Delta x = 0.1$.
- The profile of the travelling and stationary waves has amplitude $A = 0.5$.
- We set $\tau = 0$ and $\gamma = 0.5$.
- The non-uniform electrode wall used is $h(x) = 0.01(e^{-(x-40)^2} + e^{-(x+40)^2})$.
- The time mesh step is $\Delta t = 0.005$.
- We take $f = c_0 - 0.04$, where c_0 is the velocity of the travelling wave.
- The artificial sponge used is $s(x) = 5(\tanh(x + 150) - \tanh(x - 150)) - 10$.

The initial condition is chosen as $\eta(x,0) = \eta_1(x) + \eta_2(x)$, where η_1 is the travelling wave solution of the equation in the absence of a non-uniform electrode wall, and η_2 is the stationary wave solution of the equation under the effect of the non-uniform electrode wall. Figure B1 shows this evolution.

Figure B1 shows the solutions $\eta(x)$ obtained at times $t = 1550$ and $t = 8800$ for both cases with and without sponge. Note that the solutions are very close, and as time increases, they drift apart due to radiation leaving on the left and reentering from the right, causing spurious interactions that must be avoided. The solution to this issue is the use of an artificial sponge.

Figure C1 shows the relative error $E(t)$ as a function of time t in the interval $I = [-60,60]$. The behaviour is evaluated only in the interval I, since this is the region where the sponge is not expected to affect the solution. The relative error is given by

$$E(t) = \frac{\left|\left|\vec{\eta_w}(x,t) - \vec{\eta_s}(x,t)\right|\right|_2}{\left|\left|\vec{\eta_w}(x,t)\right|\right|_2}, \tag{B.2}$$

where $\vec{\eta_w}$ and $\vec{\eta_s}$ are vectors with coordinates $\eta_{w_j} = \eta_w(x_j,t)$ and $\eta_{s_j} = \eta_s(x_j,t)$, with η_w and η_s being the solutions of equation (B.1) without and with sponge, respectively, and x_j are common points in both meshes of the cases without and with sponge, such that $x_j \in (-60,60)$. The small magnitude of the relative error shows that the sponge does not affect the solution in the domain region where $s(x) \approx 0$. Note that from the very beginning, there is already a small relative error due to weak radiation that occurs from the start of the simulation.

It can be seen in the graph of Figure C that from time $t = 8000$ onwards, there is an increase in the order of the error, which agrees with what is shown in Figure B.